Optical Absorption and Valence Band Photoemission from Uncapped CdTe Nanocrystals

G. L. Tan,*,† N. Wu,‡ J. G. Zheng,‡ U. Hommerich,† and D. Temple†

Physics Department, Hampton University, Hampton, Virginia 23668, and Keck Interdisciplinary Surface Science Center, NUANCE, Northwestern University, 2200 Campus Drive, Evanston, Illinois 60208-3108

Received: October 31, 2005; In Final Form: December 8, 2005

CdTe nanocrystals have been successfully fabricated by a mechanical alloying process. X-ray diffraction (XRD) patterns demonstrate that a single-phase CdTe compound with a zinc blende structure has been formed after ball milling elemental Cd and Te mixture powders for 27 h. The large broadening effect for the width of the {111} diffraction peak of uncapped CdTe nanocrystals on smaller size was observed in slowly scanned XRD patterns. The X-ray photoelectron spectrum was used to study the surface of the uncapped CdTe nanocrystals within both core level and valence band regions. The presence of tellurium oxide film on the surface of the uncapped CdTe nanocrystals has been detected in the X-ray photoelectron spectrum of the Te 3d core level, which was comparable to the observed amorphous oxide thin layer on the surface of uncapped CdTe nanocrystals in a high resolution transmission electron microscopy (HRTEM) image. The energy of the valence band maximum for uncapped CdTe powders blue shifts to the higher energy side with smaller particle sizes. In UV−visible optical absorption spectra of the suspension solution containing uncapped CdTe nanocrystals, the absorption peaks were locating within the ultraviolet region, which shifted toward the higher energy side with prolonged ball milling time. Both blue shifts of valence band maximum energy and absorption peaks with decreasing particle size provide a unique pathway to reveal the quantum confinement effect of uncapped CdTe nanocrystals.

1. Introduction

Semiconductor quantum dots (QDs) are of great interest for both fundamental research and technical applications.[1−5] The electronic structure of semiconductor quantum dots is strongly size dependent when the dot diameter is comparable to or smaller than the Bohr exciton radius.[6] Theoretical studies of such systems have predicted many interesting effects in semiconductor cluster electronic structure including discrete well-defined states near the edge of the band.[7,8] Optical studies have confirmed these models of quantum confinement.[9−11] Valence band photoemission from CdS nanocrystals[12] also gave useful information on the quantum confinement effect in addition to the optical spectrum. The quantum confinement effect usually results in a blue shift of band gap energy, leading to strong size-dependent optical properties including band edge absorption and peak photoluminescence wavelength.[7,13−15] CdTe and CdSe nanostructures are among the best-studied semiconductor quantum systems.[16−18] Several wet chemical methods have been developed for the synthesis of monodisperse and highly crystalline CdTe,[19,20] CdS,[21,22] ZnS,[23] CdSe,[24,25] and InAs[15] nanocrystals, whose surface was modified by organic coating ligands. During wet chemical processing, the passivation of nanocrystals by long chain organic surfactants, such as trioctylphosphine oxide (Tech TOPO) and alkylamines, is essential in order to disperse and stabilize nanocrystals in the solvent.[26] A dry physical route has also been reported recently for the synthesis of CdTe nanocrystals by mechanical alloying as well as a subsequent trioctylphosphine/trioctylphosphone oxide (TOP/TOPO) modifying technique.[27,28]

The dry physical route provides a way to prepare uncapped CdTe nanocrystals, which may exclude the chemical interaction effect between the surface of nanoparticles and the modifying organic ligand.[27] It has long been believed that the surface effect of small nanocrystals (NCs) plays an important role on optical performance as well as carrier relaxation and recombination processes.[29−33] Since nanocrystals possess a large surface-to-volume ratio, their optical properties are generally related to the surface structure. Hence, it makes sense to investigate the influence of the growth process on the surface status and, more interestingly, the influence of the surface status on the nanocrystals' optical properties. A widely used method for surface probing is X-ray photoelectron emission spectroscopy.

Investigations of CdS,[21,22] ZnS,[23] CdSe,[24,25] and InAs[26] are some examples for surface structure studies of semiconductor nanocrystals by high resolution photoelectron spectroscopy. Furthermore, composite nanocrystals such as CdSe/ZnS[24] core−shell or CdS/HgS/CdS[34] quantum well nanostructures have been studied by synchrotron X-ray photoelectron spectroscopy (XPS). We have conducted a photoemission study on the uncapped CdTe nanocrystals, aiming to reveal if there is any performance difference on the surfaces of nanocrystals of varying sizes, which might help to explain the observed blue shifts in their optical band gap energies. Under this consideration, we have measured the linear optical properties, that is, the UV−visible absorption spectrum upon the dispersion solution of uncapped CdTe nanocrystals, the results of which were then compared with the valence band XPS spectrum to reveal the changes in electronic structure of uncapped CdTe nanocrystals with varying particle size.

2. Experimental Method

The starting powder mixtures of high purity cadmium (99.99%) and tellurium (99.999%) elemental powder were sealed in a hardened steel vial with hardened steel balls. Milling

* Corresponding author. E-mail: gltann@yahoo.com.
† Hampton University.
‡ Northwestern University.

10.1021/jp056289u CCC: $33.50
Published on Web 01/17/2006

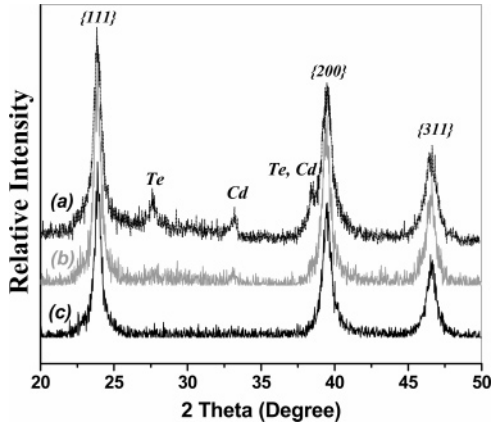

Figure 1. XRD pattern for the self-propagation reaction of elemental Cd and Te powder as a function of ball milling time.

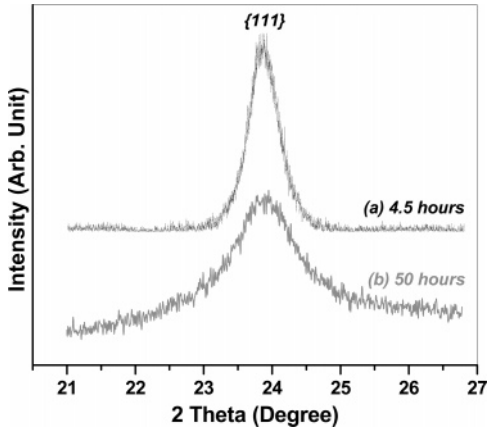

Figure 2. X-ray diffraction peak from the {111} lattice plane for CdTe nanocrystals with zinc blende structure after ball milling for (a) 5.5 h and (b) 50 h.

balls of different diameters (2−12 mm) were used. The ball milling process was carried out with a SPEX 8000D mix/miller using a ball-to-powder mass ratio of 20:1. The stoichiometric amounts of Cd and Te elemental powder with a 1:1 atomic ratio were then mechanically alloyed to the CdTe compound after the ball milling process for a certain period of time. A small amount of uncapped powders was taken out of the vial within different intervals for structural and optical measurement. The structural phase composition of the as-milled powders was detected by a Rigaku powder X-ray diffractometer. UV−visible absorption spectra were measured in a dispersion solution of these uncapped CdTe nanocrystals in hexane.

XPS analyses were performed on the uncapped CdTe powders with an Omicron ESCA probe, which was equipped with an EA125 energy analyzer. Photoemission was stimulated by monochromated Al Kα radiation (1486.6 eV) with an operating power of 300 W. A low energy electron flood gun was employed for charge neutralization. The analyzer was operated in the constant analyzer energy (CAE) mode at 50 and 25 eV for survey scan and detailed scan of core level lines, respectively. The takeoff angle was set at 45°. Prior to XPS measurement, the powders were pressed to form a pellet, which was then put into the entry-load chamber to pump overnight. In addition, XPS measurement was also carried out on the bulk CdTe single-crystalline sample for comparison. To calibrate the XPS instrument, the Fermi energy of a pure gold sample was determined. All binding energies of the spectra were referenced to the Fermi energy of pure gold.

3. Results and Discussion

3.1. X-ray Diffraction Patterns. Cadmium and tellurium elemental powders were mixed together in stainless steel vials and mounted on a SPEX 8000D ball milling machine. CdTe nanocrystals were synthesized via the solid-state reaction of Cd + Te → CdTe under high frequency impacting the mixture powders from hardened alloy balls against the wall. The crystal structure of the mechanically alloyed products was identified using an X-ray powder diffractometer.

Figure 1 shows the X-ray diffraction patterns for the products of mechanical alloying elemental Cd and Te powders after ball milling for 2, 4.5, and 27 h. The detailed structural evolution of the ball milling mixture powders has been described elsewhere.[27] However, here, it is worth mentioning that, after ball milling for 2 h, most of the elemental Cd and Te powder was transformed into a CdTe compound; only a small amount of elemental Te and Cd powders was traced, as shown in Figure 1a. When the ball milling time was prolonged to 4.5 h, the diffraction peaks from zinc blende CdTe became dominant while the signals of elemental phases became subtle, as shown in Figure 1b. After mechanical alloying of the mixture of elemental powders of Cd and Te for 27 h, all X-ray diffraction (XRD) peaks from elemental Cd and Te disappeared (Figure 1c) and only three main diffraction peaks corresponding to the {111}, {200}, and {311} lattice planes of cubic CdTe were detected, indicating that single-phase CdTe powders with zinc blende structure have been fabricated, being consistent with the conclusion drawn from high resolution transmission electron microscopy (HRTEM) observation.[27]

3.2. Diffraction Peaks from the {111} Lattice Plane. To estimate the average size of uncapped CdTe nanocrystals, the {111} peak was rescanned upon the RIGAKU X-ray machine to improve peak quality at a slower angle scanning speed mode (0.002°/step) within the 2θ angle range 21−27°. In this way, more data points in smaller steps were collected, such that the Scherer equation ($d = \kappa\lambda/(\beta \cos \theta)$, where d is the diameter of the nanocrystals, λ is the wavelength of the X-ray beam, β is the full width at half-maximum (fwhm) height of the diffraction peak, and θ is the diffraction angle) could be applied to estimate the particle sizes from the XRD patterns with higher accuracy. The results are exhibited in Figure 2, where it is clearly seen that the fwhm of the {111} diffraction peak from the uncapped CdTe powder ball milling for 50 h is much wider than that from the sample ball milling for 4.5 h. The broadening {111} diffraction peak indicates a much higher ratio of smaller particles formed in the longer ball milling products. According to the Scherer equation, the average particle size was estimated to be 3.5 nm for the 50 h sample and 23 nm for the 4.5 h one.

3.3. HRTEM Image of the Uncapped CdTe Nanocrystals. Figure 3 shows a HRTEM image of CdTe powder ball milling for 27 h. No surface modification by long chain organic molecules on these as-milled CdTe powders has been made. Lattice fringes on the TEM micrograph indicate that these CdTe particles are crystalline. Figure 3 shows aggregation of several uncapped CdTe nanoparticles (A, B, C) with one-dimensional lattice fringes, which is assigned to being a cubic structure with [011] orientation. The lattice parameter was determined to be 6.48 Å, being consistent with the bulk value of cubic CdTe. Because the electron beam is not parallel to the low zone axes of the particles in most cases, it is impossible to see two-dimensional images in every particle without tilting the specimen. However, one-dimensional lattice fringes with marked {111} interplanar spacing are readily seen, as shown in Figure 3. This fact suggests that the uncapped particles are cubic CdTe,

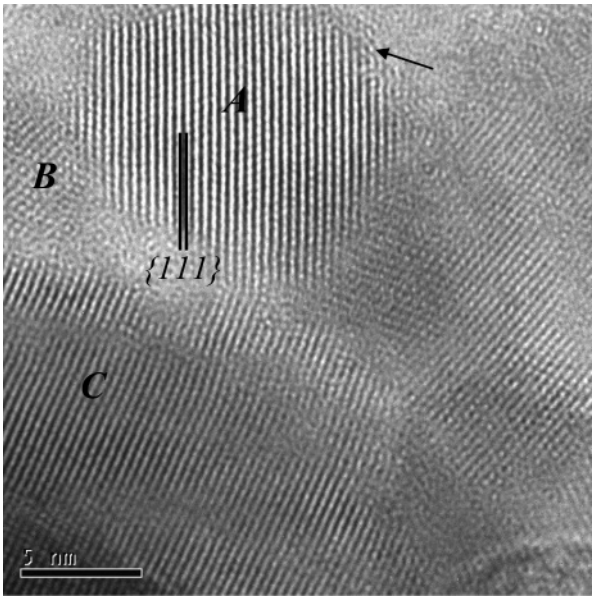

Figure 3. HRTEM images of uncapped CdTe nanocrystals after ball milling for 27 h.

which is consistent with the conclusion drawn from X-ray diffraction. A thin layer of amorphous oxide on the surface of particle A, which is indicated by an arrow, shows up in Figure 3.

Figure 3 also reveals the fact that the small crystalline particles often aggregate, which makes it impossible to show individual particles in a lower magnification TEM micrograph and obtain a quantitative particle size distribution. Small particles of a few nanometers were frequently observed in the as-milled samples, such as particle A with a size of 8 nm. However, particle size may range from a few nanometers to a few tens of nanometers. Low magnification TEM images for the CdTe nanocrystals being modified on the surface by TOP/TOPO molecules has been reported elsewhere,[27] where a homogeneous size distribution for those surface-modified CdTe nanocrystals in suspension solutions has been observed within the size range 1.5−6 nm.

3.4. XPS Study on the Surface Performance of Uncapped CdTe Nanocrystals. *3.4.1. Te 3d Core Level.* Figure 4 shows the XPS spectra of the Te 3d core level obtained from the uncapped CdTe powders as well as the bulk CdTe single-crystalline sample. All of the Te 3d spectra of the uncapped samples displayed two pairs of spin−orbit doublet components. The doublet component with a higher binding energy (Te $3d_{5/2}$ at 576.2 eV and Te $3d_{3/2}$ at 586.6 eV) was in agreement with the reported values from Te−O bonding.[35−38] The Te $3d_{5/2}$ and Te $3d_{3/2}$ peak positions of bulk CdTe are centered approximately at 572.3 and 582.5 eV, respectively, while the corresponding peak positions of TeO_2 are centered approximately at 576.2 and 586.6 eV, respectively. The observed shift of the 3.9 eV peak to higher energy for the Te $3d_{5/2}$ energy levels of uncapped CdTe nanocrystals relative to bulk values is the result of electron density transfer from tellurium to oxygen, being consistent with the corresponding shift value of 3.7 eV reported in the literature.[39] This undoubtedly indicated the presence of tellurium oxide film on the surface of uncapped CdTe powders, which confirms the observed thin layer of amorphous oxide on the surface of uncapped CdTe nanocrystals in the HRTEM image in Figure 3. Oxidation on the surface of CdSe and CdTe nanocrystals is well-known. Even under ambient conditions (without intense excitation), surface oxidation of CdTe and CdSe

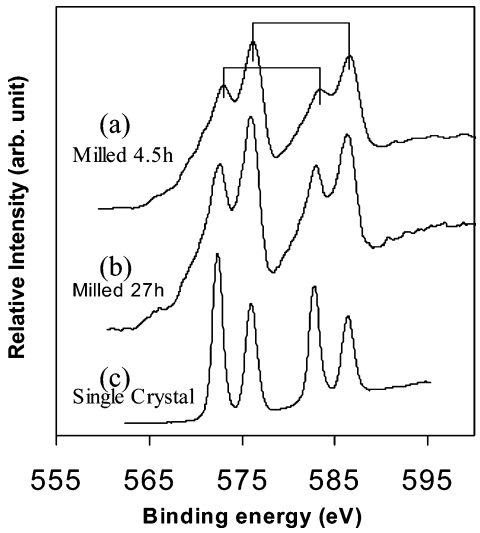

Figure 4. XPS spectra of the Te 3d core level of the uncapped CdTe nanocrystals after ball milling for (a) 4.5 h and (b) 27 h as well as (c) bulk CdTe crystal.

TABLE 1: Binding Energies for the Core Levels of Te and Cd in Uncapped CdTe Powders as well as the Single-Crystalline Sample

sample	Te $3d_{5/2}$ (eV) (Te−Cd bond)	Te $3d_{5/2}$ (eV) (Te−O bond)	Cd 4d (eV)
powder milled for 4.5 h	572.9	576.2	11.4
powder milled for 27 h	572.3	576.2	11.0
bulk CdTe crystal	572.3	576.1	11.0

nanocrystals may happen due to the chemical absorption of oxygen after exposure to air for several hours[35,40] and has been reported in several works.[39,41,42] The main oxidation product was suggested to be TeO_2 and SeO_2, respectively,[31,35,42] which was in agreement with our observed oxide thin layer on the surface of uncapped CdTe nanocrystals. In Figure 4, the Te 3d doublet component with a lower binding energy was characteristic of Te−Cd bonding. The Te $3d_{5/2}$ peak for the 4.5 h sample locates at 572.9 eV (Figure 4a), which moves down to 572.3 eV for the 27 h sample (Figure 4b), being at the same position as that observed in the bulk CdTe single-crystalline sample. The binding energies of core levels for Te and Cd are summarized in Table 1.

Therefore, it may be elucidated that single-phase CdTe nanocrystals have been formed after mechanical alloying Cd and Te elemental powders for 27 h, which has been confirmed by XRD patterns, XPS spectra, and HRTEM images. The process of mechanical alloying deduces the charge transfer as well as the chemical interaction between Cd and Te atoms during the ball milling process, leading to the chemical shift of the Te $3d_{5/2}$ and Te $3d_{3/2}$ peaks from the value of elemental Te toward the value of the CdTe compound. It thus confirms reversely with XPS results that the 27 h ball milling CdTe sample has the same crystal structure as the bulk single-crystal counterpart. Meanwhile, the 4.5 h uncapped powders are still composed of a mixture of the CdTe compound as well as a small trace of Cd and Te elemental powders, which was probably one of the factors causing the 0.4 eV chemical shift for the Te $3d_{5/2}$ peak in the 4.5 h sample.

3.4.2. Cd 4d Valence Level. Figure 5 demonstrates the XPS spectra of the Cd 4d energy level for uncapped ball milling CdTe powders as well as the bulk CdTe single-crystalline sample. The Cd 4d spectrum of the powder sample ball milling for 4.5 h presented a peak at 11.4 eV. This peak shifted to 11.0 eV after the 27 h ball milling process, which was in agreement

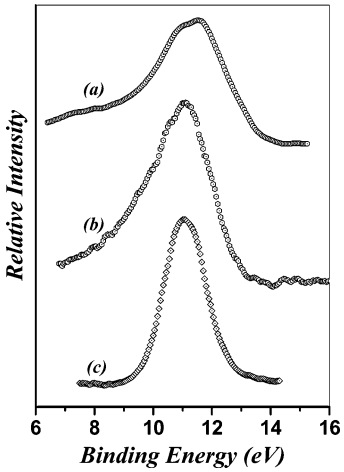

Figure 5. XPS spectra of the Cd 4d level for uncapped CdTe powders after ball milling for (a) 4.5 h and (b) 27 h as well as (c) bulk CdTe single crystal.

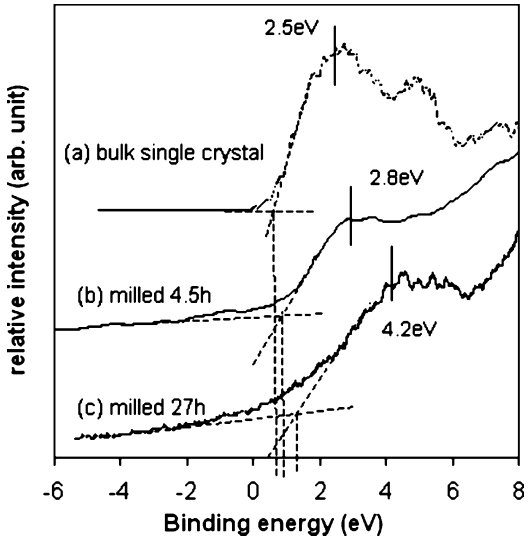

Figure 6. XPS valence band spectra for bulk CdTe crystal (a) as well as uncapped CdTe nanocrystals (b) after ball milling for 4.5 h and (c) after ball milling for 27 h.

with the corresponding position of the Cd 4d peak for the bulk CdTe single-crystalline sample as well as the value reported in the literature.[43] Since this energy is a little far away from the band gap region of CdTe, the binding energy of the Cd 4d level peaks should not be affected by the quantum confinement effect and therefore stays stable with varying particle size, as shown in Figure 5. A chemical shift of 0.4 eV for the Cd 4d level occurred in the 4.5 h uncapped CdTe powders in comparison with bulk CdTe, which was potentially resulting from the impurity elements in this sample.

On the basis of the results of the XPS and XRD measurements, most of the chemical interaction (charger transfer) between Cd and Te was completed after 4.5 h of ball milling. However, the solid-state reaction (Cd + Te → CdTe) was not completely finished, with a small trace of remnant Cd and Te components being indexed from its XRD pattern. This impurity leads to a chemical shift of 0.4 eV in the Cd 4d level. It is well-known that the solid-state reaction progresses gradually during the ball milling process.[44,45] With longer ball milling time, interdiffusion of Cd and Te proceeded, leading to the change in the coordination of Cd and Te. In addition, ball milling induced severe internal strain, defects, and a large area of grain boundaries. Keeping this in mind, it is not surprising that the Te 3d and Cd 4d peaks shifted with longer ball milling time. After 27 h of milling, the reaction (Cd + Te → CdTe) was completed and consequently the powder was composed of single-phase CdTe nanocrystals, which shares the same structure with its bulk counterpart.

3.4.3. Valence Band Structure. Figure 6 shows the valence band XPS spectra obtained from the uncapped CdTe powders through the ball milling process as well as from the bulk CdTe crystalline sample. For the bulk CdTe single-crystalline sample, the signal intensity maximum at the upper tail of the band edge occurred at 2.5 eV, which was close to the reported value of 2.4 eV.[44,46] The signal intensity maximum of the CdTe powders after ball milling for 4.5 h is located at 2.8 eV, and it moves further toward the higher energy side at 4.2 eV after ball milling for 27 h, as shown in Figure 6. The whole valence band edge in XPS spectra of uncapped CdTe nanocrystals shifted to the higher binding energy side with prolonged ball milling time, in comparison with that of the bulk CdTe single-crystalline sample. The longer the ball milling time, the more smaller particles are formed in the mixture powders, leading to a bigger blue shift of the valence band edge.

By definition, the intercept of the linear extrapolation of the leading band edge with the energy axis represents the valence band maximum.[12,47,48] However, the titled baselines at the lower energy tail of the valence band edge for nanometer powders are not parallel to the energy axis, so we took the intercept of the linear extrapolation of the leading valence band edge with the baselines instead of the energy axis to represent the valence band maximum. For the single-crystalline sample, it makes no difference for either choice. The valence band maximum points upon interception of the sharp band edge with the energy axis for the bulk CdTe crystal are shown in Figure 6a, while those upon intercept of the leading edge with the tilted baseline are shown in Figure 6b and c with dashed lines for the 4.5 and 27 h CdTe nanocrystals, respectively. In this way, the valence band maximum energies were determined to be 0.7 eV for the bulk CdTe crystal, 1.0 eV for the 4.5 h uncapped CdTe powders, and 1.45 eV for the 27 h uncapped CdTe nanocrystals. From Figure 6, it is evident that as the nanocrystal becomes smaller the valence band maximum energy shifts to a higher binding energy. The magnitude of this shift is 0.75 eV between the bulk CdTe single crystal and the 27 h uncapped CdTe nanocrystals. This effect is not a translation of the entire spectrum, as would be the case with band bending, but rather, it manifests itself as a change in the slope of the photoemission threshold.[12] This effect is due to changes in the electronic structure of the uncapped CdTe nanocrystals.

There is a small but measurable blue shift in the valence band maximum energy in smaller particles from prolonging milling time. The magnitude of the blue shift in valence band maximum depends on quantum confinement as well as the ability of the dots to stabilize the positive hole left behind by the photoemission.[43] This shift of valence band maximum away from the Fermi energy suggests a narrowing of the valence bandwidth with smaller particle size (longer ball milling time), thus resulting in the enlargement of band gap energies. Therefore, the blue shift of the valence band maximum energy correlates well with the optical measurements of band gap broadening. Such valence band XPS spectra give complimentary information to the quantum confinement effect of semiconductor nanocrystals in addition to the optical studies.[27] If we assume that the Fermi energy locates at the center of the band gap, double valence band maximum values may roughly represent the band gap energies. For example, from Figure 6, the valence band

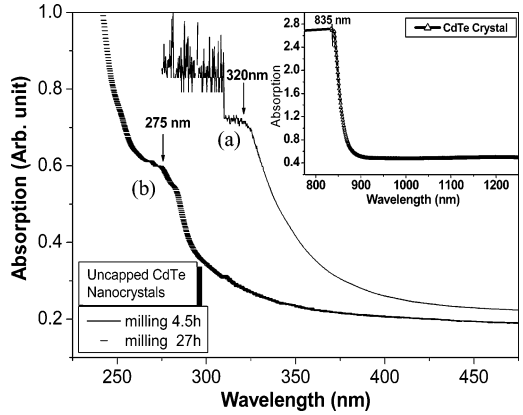

Figure 7. UV−visible absorption spectra for the suspension solution of uncapped CdTe nanocrystals in hexane after ball milling (a) for 4.5 h and (b) for 27 h. The absorption spectrum for the CdTe single-crystalline sample is shown in the inset.

maximum energy for bulk CdTe is estimated to be 0.7 eV, the double value of which is equal to 1.4 eV, approaching an optical gap energy of 1.48 eV. Similarly, double values of the valence band maximum energies for the 4.5 and 27 h uncapped CdTe nanocrystals are 2.0 and 2.9 eV, respectively, roughly representing their enlarged band gap energies.

The size-dependenct shift of the valence band maximum energy is ascribed to a combination of quantum confinement and loss of dielectric solvation energy in small clusters,[2,21] which is expressed by[49]

$$\Delta E = \frac{\hbar^2 \pi^2}{2 m_h R^2} + \frac{e^2}{2R} \cdot \bar{U} \qquad (1)$$

where m_h is the effective mass of the hole, R is the radius of the cluster, and $\bar{U}$ is the average potential over the 1S wave function of the hole in the crystallite. The two terms, one due to the kinetic energy and one due to the polarization, have the same sign. The above equation predicts that the gap energy shift increases with decreasing particle size, which interprets the blue shift of valence band maximum energies with decreasing particle size, being induced by the quantum confinement effect of semiconductor nanocrystals.

3.5. Optical Absorption of Uncapped CdTe Nanocrystals. The uncapped CdTe nanocrystals were taken from the vial at different intervals and were subsequently dispersed in hexane for optical measurement. No surface modification by long chain molecules was made. The dispersion solution was colorless. Since there were no long chain molecules (TOP/TOPO) coating the surface of the particles, they were termed as uncapped CdTe nanocrystals. Figure 7 shows the optical absorption spectra for the suspension solution containing uncapped CdTe nanocrystals after ball milling for 4.5 and 27 h, together with the absorption spectrum of the bulk CdTe crystal (shown in the upper right-hand corner). The cutoff value of the UV−visible absorption spectrum for the bulk CdTe single crystal was evaluated to be 835 nm from the absorption spectrum in the inset of Figure 7, which corresponds to the band gap energy of the bulk CdTe crystal (1.48 eV). It is worth noting that the absorption peaks of the suspension solution containing these uncapped CdTe nanocrystals were located within the ultraviolet wavelength region, which was quite different from those colorful suspensions of CdTe nanocrystals prepared by the conventional wet chemical method with absorption peaks located within the visible wavelength range.[47,50] The absorption peaks blue shifted to shorter wavelengths with increasing ball milling time (or in smaller particle size), as exhibited by Figure 7 (320 nm for the 4.5 h milled sample, 275 nm for 27 h milled sample). The band gap energy of the 27 h milled uncapped CdTe nanocrystals was thus estimated to be 4.51 eV, whereas the corresponding value of the bulk CdTe crystal was 1.48 eV. The big blue shift (3.03 eV) of the absorption peaks for the uncapped CdTe nanocrystals is due to the enlargement of the band gap, which was caused by the quantum confinement effect. This is in agreement with the valence band XPS measurements, whose valence band maximum energy blue shifts from 0.7 eV for bulk CdTe to 1.45 eV for 27 h uncapped CdTe nanocrystals, corresponding to a 1.42 eV broadening of the band gap energy. Both shifts reveal either the enlargement of the band gap energy or the changes of electronic structure for uncapped CdTe nanocrystals.

The particle size of the uncapped CdTe nanocrystals dispersed in hexane was estimated to be 2.1 nm for the 4.5 h milled sample and 1.8 nm for the 27 h milled CdTe nanocrystals, which was evaluated from the optical absorption spectrum in Figure 7 through the quantum confinement size effect formula.[51] The quantum size effect in optical absorption spectra (Figure 7) was only caused by ultrafine uncapped CdTe nanocrystals floating in organic hexane. The large particles bigger than the Bohr radius (6.8 nm) show very weak or no quantum confinement effect and should not contribute to band gap broadening of uncapped CdTe nanocrystals. This is also the reason the blue shift of the valence band maximum in XPS spectra of uncapped CdTe nanocrystals occurred, although the average particle size of the uncapped CdTe powders was estimated to be 13 nm for the 27 h sample and 23 nm for the 4.5 h sample. The optical absorption spectrum in Figure 7 reveals the quantum size effect only for those extremely small uncapped CdTe nanocrystals dispersing in hexane, which shows a much bigger blue shift than the valence band maximum value in the XPS spectrum for uncapped CdTe nanocrystals.

4. Conclusion

Single-phase CdTe nanocrystals with zinc blende structure have been successfully synthesized through mechanical alloying of the elemental Cd and Te mixture powders for 27 h. A prominent broadening width for the {111} diffraction peak with ball milling time or particle size was observed in the slowly scanned XRD pattern, upon which the mean particle size of uncapped CdTe nanocrystals was estimated to be 23 nm for the 4.5 h sample and 3.5 nm for the 50 h milling sample. The HRTEM image also demonstrates the formation of CdTe nanocrystals with zinc blende structure; an amorphous oxide thin layer was observed on the surface of the uncapped CdTe nanocrystals. The X-ray photoemission spectrum was employed to investigate the surface of the uncapped CdTe nanocrystals, the result of which confirms the formation of a TeO_2 thin layer on the surface of the particles. The valence band edge shifts to larger binding energies with smaller nanocrystal sizes. Big blue shifts for valence band maximum energies of these uncapped CdTe nanocrystals with decreasing particle size (ball milling time) have been observed in the valence band XPS spectrum, which corresponds to the enlargement of the band gap due to the quantum confinement effect. This was in agreement with blue shifts of the absorption peaks in the optical spectrum for the suspension solution of these uncapped CdTe nanocrystals. Therefore, the photoemission spectrum in the valence band region provides complimentary information concerning the quantum confinement effect in addition to optical studies.

Acknowledgment. The support with the XRD measurements by Dr. George Loutts at Norfolk State University is acknowledged. We are grateful to Keck-II/NUANCE, Northwestern University, for the support with the XPS and TEM measurements. One of the authors (G.L.T.) acknowledges the financial support from Shanghai Institute of Ceramics, Chinese Academy of Science.

References and Notes

(1) Brus, L. E. *Appl. Phys. A* **1991**, *53*, 465.
(2) Alivisatos, A. P. *Science* **1996**, *271*, 933.
(3) Wang, X.; Qu, L.; Zhang, J.; Peng, X.; Xiao, M. *Nano Lett.* **2003**, *3*, 1103.
(4) Peng, X.; Alivisatos, A. P. *Nature* **2000**, *404*, 59.
(5) Talapin, D. V.; Rogach, A. J.; Weller, H. *J. Phys. Chem. B* **2001**, *105*, 2260.
(6) Brus, L. E. *J. Phys. Chem.* **1986**, *90*, 2555.
(7) Kayanuma, Y. *Phys. Rev. B* **1988**, *38*, 9797.
(8) Lippens, P. E.; Lannoo, M. *Phys. Rev. B* **1989**, *39*, 10935.
(9) Hu, Y. Z.; et al. *Phys. Rev. Lett.* **1990**, *64*, 1805.
(10) Alivisatos, A. P.; et al. *J. Chem. Phys.* **1988**, *89*, 4001.
(11) Weller, H.; et al. *Chem. Phys. Lett.* **1986**, *124*, 557.
(12) Colvin, V. L.; Alivisatos, A. P. *Phys. Rev. Lett.* **1991**, *66*, 2786.
(13) Stokes, K. L.; Persans, P. D. *Phys. Rev. B* **1996**, *54*, 1892.
(14) Rogach, A. L.; Kornowski, A.; Gao, M.; Eychmuller, A.; Weller, H. *J. Phys. Chem. B* **1999**, *103*, 3065.
(15) Alivisatos, A. P. *J. Phys. Chem. B* **1996**, *100*, 13226.
(16) Weller, H. *Angew Chem., Int. Ed. Engl.* **1993**, *2*, 41.
(17) Ridley, B. A.; Nivi, B.; Jacobson, J. M. *Science* **1999**, *286*, 746.
(18) Kim, S. H.; Medeiros, R. G.; Ohlbergf, D. A. A.; Stanley, W. R.; Heath, J. R. *J. Phys. Chem. B* **1999**, *103*, 10341.
(19) Murray, C. B.; Norris, D. J.; Bawendi, M. G. *J. Am. Chem. Soc.* **1993**, *115*, 8706.
(20) Talapin, D. V.; Rogach, A. L.; Mekis, I.; Haubold, S.; Kornowski, A.; Haase, M.; Weller, H. *Colloids Surf., A* **2002**, *202*, 145.
(21) Steigerwald, M. L.; et al. *J. Am. Chem. Soc.* **1988**, *110*, 3046.
(22) Winkler, U.; Eich, D.; Chen, Z. H.; Fink, R.; Kulkarni, S. K.; Umbach, E. *Chem. Phys. Lett*. **1999**, *306*, 95.
(23) Nanda, J.; Sarma, D. D. *J. Appl. Phys*. **2001**, *90*, 2504.
(24) Borchert, H.; Talapin, D. V.; McGinley, C.; Adam, S.; Lobo, A.; Castra, A. R. B. de; Moeller, T.; Weller, H. *J. Chem. Phys*. **2003**, *119*, 1800.
(25) Li, L. S.; Hu, J.; Yang, W.; Alivisatos, A. P. *Nano Lett.* **2001**, *1*, 349.
(26) McGinley, C.; Liedler, M.; Moeller, T.; Borchert, H.; Haubold, S.; Haase, S.; Weller, H. *Phys. Rev. B* **2002**, *65*, 245308.
(27) Tan, G. L.; Hommerich, U.; Temple, D.; Wu, N. Q.; Zheng, J. G.; Loutts, G. *Scr. Mater.* **2003**, *48*, 1469.
(28) Tan, G. L.; Yang, Q.; Hömmerich, U.; Seo, J. T.; Temple, D. *Opt. Mater.* **2004**, *27*, 579.
(29) Brus, L. E. *J. Phys. Solids* **1998**, *59*, 459.
(30) Pileni, M. P. *Catal. Today* **2000**, *58*, 151.
(31) Klimov, V. I.; Mcbranch, D. W.; Leatherdal, C. A.; Bawendi, M. G. *Phys. Rev. B* **1999**, *60*, 13740.
(32) Bawendi, M. G.; Carrol, P. J.; Wilson, W. L.; Brus, L. E. *J. Chem. Phys.* **1992**, *96*, 946.
(33) Carter, A. C.; Bouldin, C. E.; Kemner, K. M.; Bell, M. I.; Woicik, J. C.; Majetich, S. A. *Phys. Rev. B* **1997**, *55*, 13822.
(34) Borchert, H.; Dorfs, D.; McGinley, C.; Adam, S.; Moeller, T.; Weller, H.; Eychmueller, A. *J. Phys. Chem. B* **2003**, *107*, 7486.
(35) Moulder, J.; Stickle, W.; Sobel, P.; Bomben, E. *Handbook of X-ray photoelectron spectroscopy*; Physical Electronics: Eden Prairie, MN, 1995.
(36) Sebastian, P. J.; Sivaramakrishman, V. *Phys. Status Solidi A* **1991**, *124*, 505.
(37) Choi, S. S.; Lucovsky, G. *J. Vac. Sci. Technol., B* **1988**, *6*, 1198.
(38) Davis, G. D.; Sun, T. S.; Buncher, S. P.; Byer, N. E. *J. Vac. Sci. Technol.* **1981**, *19*, 472.
(39) Zhang, H.; Yang, B. *Thin Solid Films* **2002**, *418*, 2002.
(40) Masson, D. P.; Lockwood, D. J.; Grahan, M. J. *J. Appl. Phys.* **1997**, *82*, 1632.
(41) Bowen, J. E.; Colvin, V. L.; Alivisatos, A. P. *J. Phys. Chem.* **1994**, *98*, 4109.
(42) Aldana, J.; Wang, Y. A.; Peng, X. *J. Am. Chem. Soc.* **2001**, *123*, 8844.
(43) Borchert, H.; Talapin, D. V.; Gaponik, N.; McGinley, C.; Adam, S.; Lobo, A.; Moeller, T.; Weller, H. *J. Phys. Chem. B* **2003**, *107*, 9662.
(44) Sherif, M.; Eskandarany, E. L.; Sumiyama, K.; Suzuki, K. *J. Mater. Res.* **1995**, *10*, 659.
(45) Kosmac, T.; Maurice, D.; Courtneym, T. H. *J. Am. Ceram. Soc.* **1993**, *76*, 2345.
(46) Sherif, M.; Eskandarany, E. L.; Sumiyama, K.; Suzuki, K. *J. Mater. Res.* **1995**, *10*, 659.
(47) Hansen, J. C.; Wagner, M. W.; Tobin, J. G. *Solid Sate Commun.* **1989**, *72*, 319.
(48) Boieriu, P.; Sporken, R.; Sivananthan, S. *J. Vac. Sci. Technol., B* **2002**, *20*, 1777.
(49) Brus, L. E. *J. Chem. Phys.* **1984**, *80*, 4403.
(50) Brennan, J. G.; Siegrist, T.; Caeeol, P. J.; Stucznski, S. M.; Reynders, P.; Brus, L. E.; Steigerwald, M. L. *Chem. Mater*. **1990**, *2*, 403.
(51) Manna, L.; Yang, W.; Wickham, J.; Scher, E.; Kadavanich, A.; Alivisatos, A. P. *Nature* **2000**, *404*, 59.